Source Localization Using Matched-Phase Matched-Field Processing With Phase Descent Search

Teyan Chen, Chunshan Liu, and Yuriy V. Zakharov, *Senior Member, IEEE*

***Abstract*—The matched-phase coherent broadband matched-field (MF) processor has been previously proposed and shown to outperform other advanced broadband MF processors. It has been previously proposed to search the matched phases using the simulated annealing, which is well known for its ability of solving global optimization problems while having high computational complexity. This prevents simultaneous processing of many frequencies, and thus, limits the processor performance. We propose to use a novel iterative technique, the phase descent search (PDS), for searching the matched phases. This technique is based on coordinate descent optimization which is mainly applicable to solving convex problems. In this work, we investigate its application to the phase search problem, which is a nonconvex problem. We show that the PDS algorithm obtains matched phases similar to that obtained by the simulated annealing, and has significantly lower complexity. Therefore, it enables to search phases for a large number of frequencies and significantly improves the processor performance. The proposed processor is applied to real data from the 1996 Shallow Water Experiment (SWellEx-96) for locating a moving acoustic source at distances between 1 and 9 km with a step of about 150 m. At each distance, one 1-s snapshot with 13 frequencies is enough to provide accurate localization of the source well matched to global positioning system (GPS) measurements.**

***Index Terms*—Broadband processor, matched-field processing (MFP), matched-phase coherent processor, phase descent search (PDS).**

I. Introduction

MATCHED-FIELD PROCESSING (MFP) [1] has been widely used in ocean acoustic applications, such as source localization [2], [3] and estimation of ocean parameters [4], [5]. For locating an acoustic source, the MFP computes a set of modeled acoustic fields, "replicas," at a hydrophone array. Each replica is produced for a particular source location in the underwater environment of interest. The measured acoustic field, "data," collected by the real hydrophone array is then matched with each of the replicas. This produces an ambiguity surface, which shows the correlation between each of the replicas and the data. The peak in the ambiguity surface should indicate the true source position, where the replica and the data are well correlated, providing that the propagation model used to generate the replicas is accurate.

Manuscript received June 04, 2010; revised October 30, 2011; accepted December 16, 2011. Date of publication February 10, 2012; date of current version April 13, 2012. A part of this material has been presented at the European Conference on Underwater Acoustics (ECUA), Istanbul, Turkey, July 2010.

Associate Editor: R. Chapman.

The authors are with the Department of Electronics, University of York, York YO10 5DD, U.K. (e-mail: tc512@york.ac.uk; cl563@ohm.york.ac.uk; yz1@ohm.york.ac.uk).

Color versions of one or more of the figures in this paper are available online at http://ieeexplore.ieee.org.

Digital Object Identifier 10.1109/JOE.2011.2181269

Broadband (or multifrequency) MFP has been actively investigated in the past two decades [2], [6]–[10]. Coherent combining of ambiguity surfaces obtained at different frequencies provides better performance compared to incoherent combining. In scenarios where an acoustic source transmits sound at multiple frequencies, phases of the source frequencies contribute in the measured acoustic data. The phase shifts between different frequencies should be compensated before the MFP; however, they are often unknown. To compensate for these phase shifts, a matched-phase coherent processor was proposed [10]. This processor has been shown to outperform other advanced MF processors, especially when the ambient noise level and environment mismatch are significant [10]. A cross-frequency processor, which can be seen as an incoherent version of the matched-phase processor, is then proposed in [11]; it has been shown that this processor provides similar maximum of the ambiguity surface as the matched-phase coherent processor.

In [10], it was proposed to search the phase shifts by using the simulated annealing algorithm, which is well known for its ability of solving global optimization problems while having high computational complexity. Although different approaches have been proposed to reduce the complexity [12], [13], it is still very high and increases dramatically as the number of free parameters increases. This prevents simultaneous processing of many frequencies, and thus, limits the processor performance. Furthermore, for most of the simulated annealing methods, it is found to be exhausting to determine some algorithm parameters such as the initial temperature and the cooling schedule, which need to be carefully set. For all these reasons, we propose to search the matched phases by using a novel iterative technique, the phase descent search (PDS) algorithm [14], which is based on coordinate descent iterations with respect to the unknown phases and constrains the solution to have a unit magnitude. Since coordinate descent optimization is mainly applicable to solving convex problems, it is not clear how it will behave in application to the phase search problem, which has been considered as a global optimization problem [10]. In this work, we investigate the application of the PDS algorithm to this problem and show that it can obtain matched phases similar to that obtained by the simulated annealing. The PDS algorithm has significantly lower complexity as compared with simulated annealing methods, and thus, enables searching matched phases for a large number of processed frequencies. This can significantly improve the processor performance. In addition, the PDS algorithm is easy to implement since all the algorithm parameters can be easily chosen.

For localization of a fast moving acoustic source, which transmits sound at multiple frequencies, the received signal suffers

from the Doppler effect. Frequency correction is required in such case, to capture the information on the shifted transmission frequencies before applying MFP. In this work, we employ a frequency estimator with dichotomous search of periodogram peak [15] for estimating the transmitted frequencies in the received data. Due to the fast movement of the source, to achieve accurate localization at each instant, a short data record (a few short snapshots) has to be used for MFP. Thus, the ability of an MF processor to solve the localization problem with a short data record is very important. We apply the proposed MF processor to the data collected in the 1996 Shallow Water Experiment (SWellEx-96) using as short as 1-s snapshots, and show accurate localization results.

The paper is organized as follows. In Section II, the data model is described. In Section III, the matched-phase coherent MF processor is introduced and the cross-frequency incoherent processor is reviewed. The PDS algorithm and the frequency estimation technique are introduced in Sections IV and V, respectively. Application of the proposed processor to experimental data is presented in Section VI. Finally, Section VII gives conclusions.

Notations: In this paper, we use capital and small bold fonts to denote matrices and vectors, respectively. For example, $\mathbf{R}$ and $\mathbf{d}$ represent a matrix and a vector, respectively. Elements of the matrix and vector are denoted as $R_{m,n}$ and d_i. A pth column of $\mathbf{R}$ is denoted as $\mathbf{R}^{(p)}$; $\mathbf{d}^H$ is the Hermitian transpose of the vector $\mathbf{d}$; $\mathrm{diag}\{\mathbf{R}\}$ denotes a vector whose entries are diagonal elements of $\mathbf{R}$. Other notations used throughout this paper are defined when considered.

II. Data Model

We consider a single acoustic source transmitting sound at multiple frequencies, and the source position can be characterized by range and depth. The data model for the signal received by the ith hydrophone of an M-hydrophone array at frequency ω is given by

$$d_i(\omega) = h_i(\omega)s(\omega) + e_i(\omega) \tag{1}$$

where $d_i(\omega)$ is the measured acoustic pressure, $h_i(\omega)$ is the channel transfer function, $s(\omega)$ is the source signal, and $e_i(\omega)$ is a zero-mean stochastic process representing additive observation noise. We can define vectors $\mathbf{h}(\omega) = \{h_i(\omega)\}_{i=1}^M$ and $\mathbf{e}(\omega) = \{e_i(\omega)\}_{i=1}^M$ for the channel transfer function and the additive observation noise, respectively. The data model can then be represented by

$$\mathbf{d}(\omega) = \mathbf{h}(\omega)s(\omega) + \mathbf{e}(\omega) \tag{2}$$

where $\mathbf{d}(\omega) = \{d_i(\omega)\}_{i=1}^M$ is a "data" vector containing the measured acoustic pressure field at the M-hydrophone array. We also define a complex-valued "replica" vector $\mathbf{p}(\omega, \mathbf{x}) = \{p_i(\omega, \mathbf{x})\}_{i=1}^M$, which contains the modeled acoustic pressure field at the M-hydrophone array, where $p_i(\omega, \mathbf{x})$ is a modeled solution to the acoustic wave equation at the ith hydrophone for a source located at $\mathbf{x}$ and transmitting acoustic signal at frequency ω.

III. Broadband Matched-Field Processing

In this section, we review the single-frequency Bartlett processor and its extension dealing with multiple frequencies, the multifrequency coherent processors. Then, the matched-phase coherent processor which requires searching the phases of the replica is considered, and an alternative expression of its ambiguity function is derived. Finally, the incoherent version of this matched-phase processor called the cross-frequency incoherent processor is also considered, which does not require any phase search.

A. Matched-Phase Coherent Processor

The single-frequency Bartlett processor is an MF processor which averages the projection of the data vectors $\mathbf{d}(\omega)$ at radial frequency ω on the normalized replica vector $\mathbf{u}(\omega, \mathbf{x}) = \mathbf{p}(\omega, \mathbf{x})/|\mathbf{p}(\omega, \mathbf{x})|$ at radial frequency ω and spatial coordinate $\mathbf{x}$. It produces the ambiguity function [6]

$$B_B(\omega, \mathbf{x}) = \frac{\left\langle \left| \mathbf{d}^H(\omega)\mathbf{u}(\omega, \mathbf{x}) \right|^2 \right\rangle_T}{tr\left[\mathbf{D}(\omega)\right]} \tag{3}$$

where we denote $\langle \cdots \rangle_T$ as the time average, $tr[\mathbf{A}]$ as the trace of a matrix $\mathbf{A}$, and $\mathbf{D}(\omega) = \langle \mathbf{d}(\omega)\mathbf{d}^H(\omega) \rangle_T$. By defining a normalized covariance matrix $\mathbf{K}(\omega) = \mathbf{D}(\omega)/tr[\mathbf{D}(\omega)]$, (3) can be written as

$$B_B(\omega, \mathbf{x}) = \mathbf{u}^H(\omega, \mathbf{x})\mathbf{K}(\omega)\mathbf{u}(\omega, \mathbf{x}). \tag{4}$$

In [10], the coherent broadband MF processor is defined based on the single-frequency Bartlett processor (4) but taking into account the nonzero phase difference between frequencies. It is given by [10]

$$\begin{aligned} B_C(\mathbf{x}) &= \left\langle \left| \frac{1}{L} \sum_{n=1}^{L} \frac{\mathbf{d}^H(\omega_n)\mathbf{u}(\omega_n, \mathbf{x})}{\sqrt{tr\left[\mathbf{D}(\omega_n)\right]}} e^{j\hat{\phi}_n} \right|^2 \right\rangle_T \\ &= \frac{1}{L^2} \sum_{m,n=1}^{L} \mathbf{u}_m^H \mathbf{K}_{m,n} \mathbf{u}_n e^{j(\hat{\phi}_n - \hat{\phi}_m)} \end{aligned} \tag{5}$$

where

$$\mathbf{K}_{m,n} = \mathbf{K}(\omega_m, \omega_n) = \frac{\left\langle \mathbf{d}(\omega_m)\mathbf{d}^H(\omega_n) \right\rangle_T}{\sqrt{tr\left[\mathbf{D}(\omega_m)\right]}\sqrt{tr\left[\mathbf{D}(\omega_n)\right]}} \tag{6}$$

and $\mathbf{u}_n = \mathbf{u}(\omega_n, \mathbf{x})$. Here the phase estimates $\hat{\boldsymbol{\phi}} = \left\{\hat{\phi}_n\right\}_{n=1}^L$ are given by

$$\hat{\boldsymbol{\phi}} = \arg\max_{[\mathbf{x}, \boldsymbol{\phi}]} \left\{ \sum_{m,n=1}^{L} \mathbf{u}_m^H(\mathbf{x}) \mathbf{K}_{m,n} \mathbf{u}_n(\mathbf{x}) e^{j(\phi_n - \phi_m)} \right\} \tag{7}$$

where $\boldsymbol{\phi} = \{\phi_n\}_{n=1}^L$. Equation (5) can be divided into two terms as

$$\begin{aligned} B_C(\mathbf{x}) = \frac{1}{L^2} \Bigg[&\sum_{m=1}^{L} \mathbf{u}_m^H \mathbf{K}_{m,m} \mathbf{u}_m \\ &+ \sum_{m \neq n}^{L} \mathbf{u}_m^H \mathbf{K}_{m,n} \mathbf{u}_n e^{j(\hat{\phi}_n - \hat{\phi}_m)} \Bigg] \end{aligned} \tag{8}$$

where the first and second terms are the summation of autofrequency components and the summation of cross-frequency components, respectively.

Although the power of interest may mostly be contributed in $B_C(\mathbf{x})$ by the autofrequency components, the noise power is also mostly contributed by these components [10], [11]. Moreover, as explained in [10], in some scenarios, the magnitude of the cross-frequency components of interest can be comparable to the magnitude of the autofrequency components. Analysis of magnitudes of autofrequency and cross-frequency components for the experiment similar to that considered in this paper has been presented in [10]. Therefore, in [10], it is proposed to use only the cross-frequency components. The processor proposed is defined according to the second term of (8)

$$B_M(\mathbf{x}) = \frac{1}{L(L-1)} \sum_{m \neq n}^{L} \mathbf{u}_m^H \mathbf{K}_{m,n} \mathbf{u}_n e^{j(\hat{\phi}_n - \hat{\phi}_m)} \tag{9}$$

where the phase terms $\hat{\boldsymbol{\phi}} = \{\hat{\phi}_n\}_{n=1}^{L}$ are estimated by using (7). It has been shown in [10] that by using only the cross-frequency components, the processor $B_M(\mathbf{x})$ has better performance than the coherent broadband processor $B_C(\mathbf{x})$, especially when the ambient noise is significant.

To find the phase terms $\hat{\boldsymbol{\phi}}$ in (7), the maximization is performed simultaneously with respect to both the phase vector $\boldsymbol{\phi}$ and the location search grid $\mathbf{x}$. It is only possible to directly search over the location grid and relative phases with sufficiently high resolution for a few frequencies ($L \leqslant 3$) [10]. For a larger number of processed frequencies, it was proposed in [10] to search the relative phases using the simulated annealing. It is well known for its ability of solving global optimization problems while having a high computational complexity; the maximum number of processed frequencies considered in [10] was five. For searching the matched phases, we propose to use a much more efficient phase search method: the PDS algorithm [14].

To apply the phase search algorithm to the matched-phase processor, we find that it is useful to derive an alternative expression for the ambiguity function of the matched-phase processor (9), which can be rewritten as

$$B_M(\mathbf{x}) = \frac{1}{L(L-1)} \left[\sum_{m,n=1}^{L} \mathbf{u}_m^H \mathbf{K}_{m,n} \mathbf{u}_n e^{j(\hat{\phi}_n - \hat{\phi}_m)} - \sum_{m=1}^{L} \mathbf{u}_m^H \mathbf{K}_{m,m} \mathbf{u}_m \right]. \tag{10}$$

We introduce a matrix $\mathbf{R}$ and a column vector $\hat{\mathbf{b}}$, whose elements are defined, respectively, as

$$R_{m,n} = \mathbf{u}_m^H \mathbf{K}_{m,n} \mathbf{u}_n \tag{11}$$

and

$$\hat{b}_n = e^{j\hat{\phi}_n}, \qquad n = 1, \ldots, L. \tag{12}$$

Equation (10) can then be expressed as

$$B_M(\mathbf{x}) = \frac{1}{L(L-1)} \left\{ \hat{\mathbf{b}}^H \mathbf{R} \hat{\mathbf{b}} - tr[\mathbf{R}] \right\}. \tag{13}$$

The phase search problem in this matched-phase processor can then be interpreted as the problem of finding a vector $\hat{\mathbf{b}}$ by maximizing the quadratic function given by the first term of (13)

$$\hat{\mathbf{b}} = \arg \max_{\mathbf{x},\mathbf{b}} \left\{ \mathbf{b}^H \mathbf{R} \mathbf{b} \right\} \quad \text{s.t. } |b_n| = 1, \qquad n = 1, \ldots, L. \tag{14}$$

B. Cross-Frequency Incoherent Processor

The cross-frequency incoherent processor proposed in [11] reduces the computational load at the cost of reducing the capability of suppressing sidelobes but still can obtain the same maximum output of B_M as the matched-phase coherent processor. Instead of searching for the matched phases over the location grid for achieving the maximum output of B_M in (9), it takes the modules of the quadratic terms across frequency, which results in

$$B_X(\mathbf{x}) = \frac{1}{L(L-1)} \sum_{m \neq n}^{L} \left| \mathbf{u}_m^H \mathbf{K}_{m,n} \mathbf{u}_n \right|. \tag{15}$$

IV. Phase Descent Search Algorithm

The PDS algorithm is based on coordinate descent iterations where coordinates are the unknown phases, and a constraint forcing the solution to have a unit magnitude. Elements of the solution vector $\mathbf{b}$ are given by

$$b_n = e^{j\phi_n}, \qquad n = 1, \ldots, L, \qquad \phi_n \in [-\pi, \pi]. \tag{16}$$

The coordinate descent iterations are applied to the phases ϕ_n and the PDS algorithm is derived by applying the dichotomous coordinate descent method [16] to the optimization problem (14) with elements b_n from (16). We can describe the PDS algorithm as shown in Table I.

The algorithm starts with initialization of the phase vector $\boldsymbol{\phi} = \boldsymbol{\phi}_0$, and finding an initial solution vector $\mathbf{b} = \mathbf{b}_0 = \exp\{j\boldsymbol{\phi}_0\}$ and residual vector $\mathbf{r} = -\mathbf{R}\mathbf{b}_0$. A step-size parameter $\beta = \beta_0$ is chosen within the interval $[0, 2\pi]$, and an index n, which denotes "successful" iterations, is set to $n = 0$.

For each $m = 1, \ldots, M_b$, the step size is reduced as $\beta \leftarrow \lambda\beta$, $0 < \lambda < 1$, and a vector $\boldsymbol{\theta}$ is computed by $\boldsymbol{\theta} = \text{diag}\{\mathbf{R}\}[1 - \cos(\beta)]$. The parameter M_b indicates the number of reductions of the step-size β. For the pth element of the solution vector $\mathbf{b}$, where p is chosen in a cyclic order ($p = 1, \ldots, L$), the element b_p might be updated as $b_{p,1} = e^{j\phi_{p,1}}$ where $\phi_{p,1} = \phi_p + \beta$, or $b_{p,2} = e^{j\phi_{p,2}}$ where $\phi_{p,2} = \phi_p - \beta$. We have $T_1 = \Re\{\Delta_1^* r_p\}$ where $\Delta_1 = b_{p,1} - b_p$, or $T_2 = \Re\{\Delta_2^* r_p\}$ where $\Delta_2 = b_{p,2} - b_p$, and $\Re\{\cdot\}$ denotes the real part of a complex number. If one of the inequalities $\theta_p > T_1$ or $\theta_p > T_2$ is satisfied, the iteration is successful, and thus, the index n is incremented; and the phase ϕ_p, element b_p, and residual vector $\mathbf{r}$ are updated as $\phi_p = \phi_{p,1}$, $b_p = b_{p,1}$, and $\mathbf{r} \leftarrow \mathbf{r} - \Delta_1 \mathbf{R}^{(p)}$, or $\phi_p = \phi_{p,2}$, $b_p = b_{p,2}$, and $\mathbf{r} \leftarrow \mathbf{r} - \Delta_2 \mathbf{R}^{(p)}$, respectively. Otherwise, they are not changed. The index n is compared with a predefined number of "successful" iterations N_u for a stopping criterion. The choice of β_0, λ, and M_b defines the final phase resolution $\beta_0 \lambda^{M_b}$; e.g., in the case of $\beta_0 = 2\pi$, $\lambda = 1/2$, and $M_b = 5$, the final phase resolution is $\pi/2^{M_b} = \pi/32$.

TABLE I
PHASE DESCENT SEARCH ALGORITHM

Step	Equation
Init.	$\varnothing = \varnothing_0$, $\mathbf{b} = \mathbf{b}_0 = \exp\{j\,\varnothing_0\}$, $\mathbf{r} = -\mathbf{R}\mathbf{b}_0$, $\beta = \beta_0$, $n = 0$
1	for $m = 1 : M_b$
2	$\beta \leftarrow \lambda\beta$
3	$\boldsymbol{\theta} = \text{diag}\,\{\mathbf{R}\}\,[1 - \cos(\beta)]$
4	Flag = 0
5	for $p = 1 : L$
6	$\varnothing_{p,1} = \varnothing_p + \beta$, $b_{p,1} = e^{j\,\varnothing\,p;1}$
7	$\Delta 1 = b_{p,1} - b_p$, $T_1 = \Re\{\Delta_1^* r_p\}$
8	if $\theta_p > T_1$
9	$n \leftarrow n + 1$, Flag = 1
10	$\mathbf{r} \leftarrow \mathbf{r} - \Delta_1 \mathbf{R}^{(p)}$
11	$\varnothing_p = \varnothing_{p,1}$, $b_p = b_{p,1}$
12	$\varnothing_{p,2} = \varnothing_p - \beta$, $b_{p,2} = e^{j\varnothing p;2}$
13	$\Delta_2 = b_{p,2} - b_p$, $T_2 = \Re\{\Delta_1^* r_p\}$
14	if $\theta_p > T_2$
15	$n \leftarrow n + 1$, Flag = 1
16	$\mathbf{r} \leftarrow \mathbf{r} - \Delta_2 \mathbf{R}^{(p)}$
17	$\varnothing_p = \varnothing_{p,2}$, $b_p = b_{p,2}$
18	end the loop over p
19	if $n > N_u$ the algorithm stops
20	if Flag = 1 go to step 4
21	end the loop over m

To solve the optimization problem (14), we define a grid of points in the range–depth plane. For each of the grid points $\mathbf{x}_k$, the PDS algorithm is used to maximize the quadratic form $\mathbf{b}^H\mathbf{R}\mathbf{b} = e^{j\boldsymbol{\phi}^H}\mathbf{R}e^{j\boldsymbol{\phi}}$, where $\mathbf{R}$ depends on $\mathbf{x}_k$ due to (11). As a result, for each point $\mathbf{x}_k$, we find the optimal phase vector $\boldsymbol{\phi}_k$ and the corresponding value of $J_k = e^{j\boldsymbol{\phi}_k^H}\mathbf{R}e^{j\boldsymbol{\phi}_k}$. We then search for k that maximizes J_k and find a solution to (14) as $\hat{\mathbf{b}} = e^{j\boldsymbol{\phi}_k}$. Finally, (13) is used to compute the ambiguity surface.

V. FREQUENCY ESTIMATION

For localization of a moving acoustic source, frequency estimation is very important. Due to the movement of the source, the received signal suffers from the Doppler effect. The frequencies received at the hydrophone array will be shifted and the shifts are usually unknown. We estimate these frequency shifts by using a frequency estimator based on the dichotomous search of the periodogram peak, which provides the performance similar to that of the maximum-likelihood estimator [15].

Since the source frequencies are transmitted simultaneously, the frequency shifts should be determined by the same compression factor η given by $\eta = \hat{f}/f_o$, where $\hat{f}$ is the received frequency and f_o is the transmitted frequency. Here, it is assumed that the compression factor is constant within a snapshot. We consider three different approaches for choosing the reference compression factor and use for MFP the one which gives the most reliable results. Fig. 1 shows the reference compression factors obtained from the data collected during SWellEx-96 by using these three approaches.

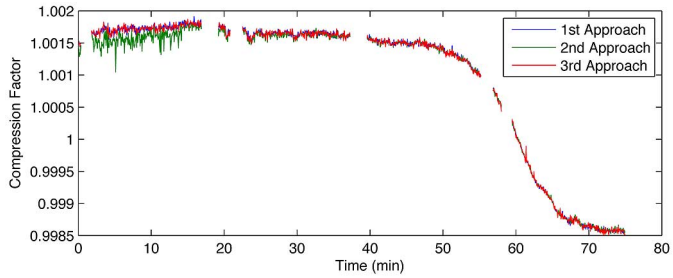

Fig. 1. Compression factors η_{ref} obtained from the data collected during SWellEx-96 by using three different approaches.

In the first approach, the frequency shifts are estimated based on the periodogram averaged over the receiver hydrophones. As a result, we obtain an L-length vector of compression factors and a vector of corresponding signal-to-noise ratios (SNRs), and denote the compression factor and the SNR for the nth frequency as η_n and SNR_n, respectively. The compression factor η_{ref} corresponding to the frequency with the highest SNR is chosen for computation of all shifted frequencies: $\eta_{\text{ref}} = \eta_{\hat{n}}$, where $\hat{n} = \arg\max_n\{\text{SNR}_n\}$.

The SNR for each estimated frequency is computed by

$$\text{SNR}_n = \left[\frac{P(\hat{f})}{\left(\frac{1}{4}\right)\sum_{k=1}^{4} P(f_k)} - 1\right] \tag{17}$$

where $P(\hat{f})$ is the signal power at the estimated frequency $\hat{f}$, and $P(f_k)$ is the power at the noise reference frequency $f_k = \hat{f} + \epsilon_k/T_s$, where $\boldsymbol{\epsilon} = [-2, -1, 1, 2]$, $k = 1, \ldots, 4$, and T_s is the length of a snapshot. The reason for using these frequencies as noise references is that they are the nearest frequencies to the estimated transmission frequencies without containing any signal information. The frequency step $1/T_s$ guarantees that frequencies f_k contain purely noise components that are not affected by the transmitted tone.

In the second approach, the frequencies are estimated based on the periodograms obtained from each receiver hydrophone. In such a case, for each snapshot, we obtain an $M \times L$ matrix of compression factors and a matrix of corresponding SNRs, and denote the compression factor and the SNR for the nth frequency at the mth hydrophone as $\eta_{m,n}$ and $\text{SNR}_{m,n}$, respectively. The reference compression factor is computed as $\eta_{\text{ref}} = \sum_{m=1}^{M}\sum_{n=1}^{L}\eta_{m,n}\ \text{SNR}_{m,n}/\text{SNR}_{\text{sum}}$, where $\text{SNR}_{\text{sum}} = \sum_{m=1}^{M}\sum_{n=1}^{L}\text{SNR}_{m,n}$.

The third approach is almost the same as the second approach, except that the reference compression factor is chosen as $\eta_{\text{ref}} = \eta_{\hat{m},\hat{n}}$, where $[\hat{m}, \hat{n}] = \arg\max_{[m,n]}\{\text{SNR}_{m,n}\}$.

According to Fig. 1, the first and third approaches provide similar results with smaller fluctuations compared to the second approach. The first approach is computationally less expensive,

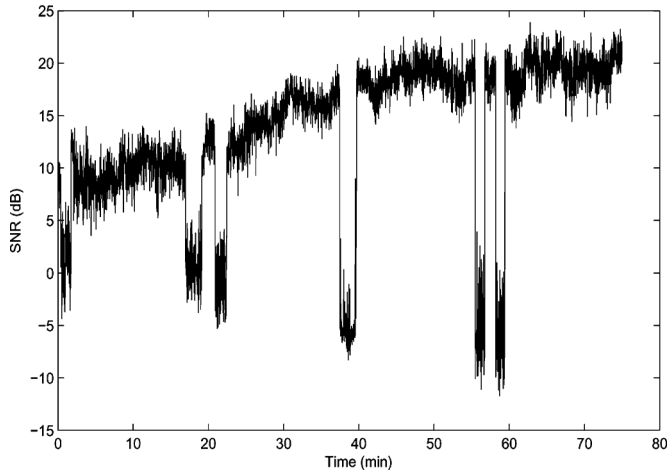

Fig. 2. SNR of the data collected at the frequency 338 Hz during the experiment.

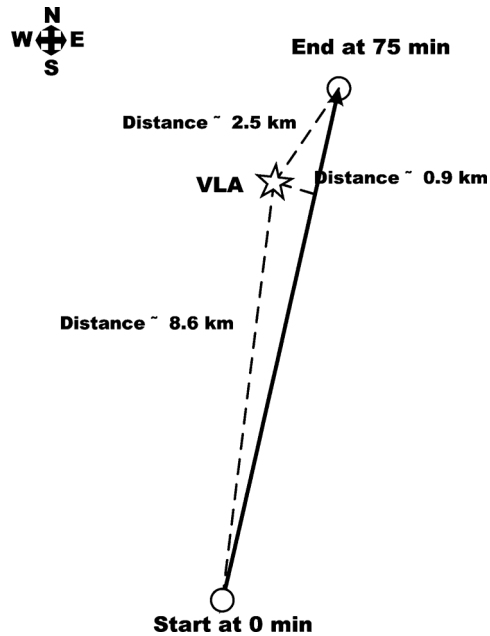

Fig. 3. Map of the source track and the location of the VLA.

and thus, is chosen to obtain the reference compression factors for our MFP analysis.

Fig. 2 shows SNR of the data collected at every 1-s snapshot for the transmission frequency 338 Hz during the experiment. We can see that, as the source is moving toward the receiver array (see Section VI-A), the SNR increases steadily from about 10 to 20 dB. As mentioned in [17], the source stopped transmitting the constant-wave (CW) tones at the beginning, midway point, and the end of the track. From Fig. 2, we can see the time periods when the source stopped transmission, which are the second, 18th to 20th, 22nd to 23rd, 39th to 40th, 57th and 60th minutes of the data collected during the experiment.

VI. Numerical Results

In this section, we present results of application of the coherent matched-phase MF processor using the proposed PDS algorithm to the data obtained in the SWellEx-96 event S5. Brief description of the experiment is first presented. Then, the coherent matched-phase MF processor using the PDS algorithm is compared with the coherent matched-phase MF processor using the simulated annealing algorithm and the cross-frequency incoherent processor.

A. Swellex-96 Event S5

SWellEx-96 was conducted in May 1996, 10 km off the coast of San Diego, CA. Details of the experiment can be found in [17]. Fig. 3 shows a map of the source track during event S5 and the location of the receiver hydrophone array, a vertical line array (VLA) used for data collection. During the experiment, a source at a supposed depth of 54 m was towed along an isobath by a source ship [17]. The source ship started its track from the south of the array and proceeded northward at a speed of about 2.5 m/s. Our analysis is based on the data collected on the VLA, which consisted of an array of 21 hydrophones with unequal depth spacing between 94.125 and 212.25 m. The sampling rate on the VLA is 1500 Hz.

The source transmitted a tonal pattern consisting of five sets of 13 tones each. Each set spanned frequencies between 49 and 400 Hz. The first set of 13 tones, which were projected at the maximum level, were used in our MFP analysis. The frequencies of the set were at 49, 64, 79, 94, 112, 130, 148, 166, 201, 235, 283, 338, and 388 Hz.

A conductivity–temperature–depth (CTD) survey was conducted during SWellEx-96 to provide the water-column sound-speed data. A sound-speed profile as recommended by [17] is used in our MFP analysis. This sound-speed profile is plotted in Fig. 4. The seafloor is modeled by three layers [17]. The first layer is a 23.5-m-thick sediment layer with an approximate density of 1.76 g/cm^3 and a compressional attenuation of about 0.2 dB/kmHz. The top and bottom of this sediment layer have compressional sound speeds of 1572.368 and 1593.016 m/s, respectively. The second layer is an 800-m-thick mudstone layer with an approximate density of 2.06 g/cm^3 and attenuation of about 0.06 dB/kmHz. The top and bottom sound speeds of the mudstone layer are 1881 and 3245 m/s, respectively. The third layer is modeled as a half-space with a density of 2.66 g/cm^3, attenuation of 0.02 dB/kmHz, and sound speed of 5200 m/s.

B. MFP Analysis

In this analysis, the program KRAKEN [18] implementing the normal mode method was employed to compute the replicas with a resolution of 10 m in range and 1 m in depth. The three-layer seafloor model as described in Section VI-A and the sound-speed profile in Fig. 4 were used for computation of the acoustic field. The data were divided into snapshots and only one snapshot was used in the MFP.

The matched-phase coherent processor (13) using the PDS algorithm was investigated. The PDS algorithm with $\lambda = 1/2$, $M_b = 5$, $\boldsymbol{\phi}_0$ with all elements equal to 0, $\mathbf{b}_0$ with all elements equal to 1, was applied for searching the matched phases. We also tried to use different initialization for the vector $\boldsymbol{\phi}_0$ and obtained the same results as presented below with similar computation time.

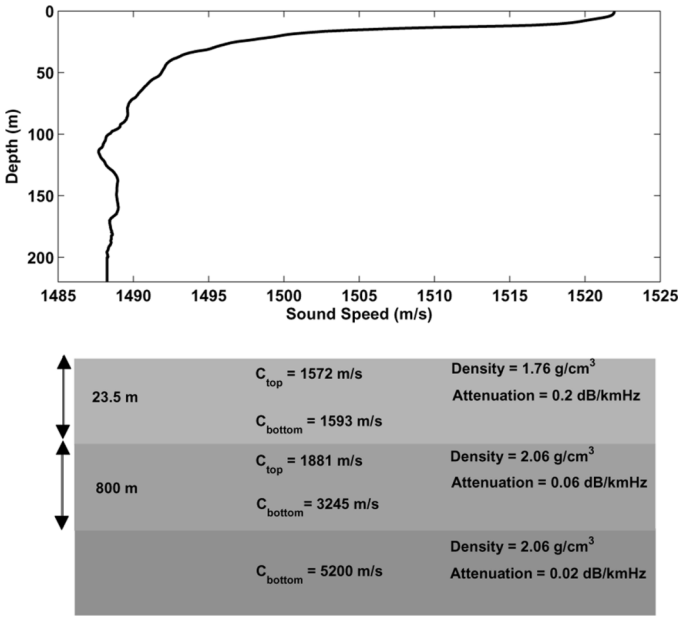

Fig. 4. Sound speed as a function of depth generated from the local CTD cast during SWellEx-96.

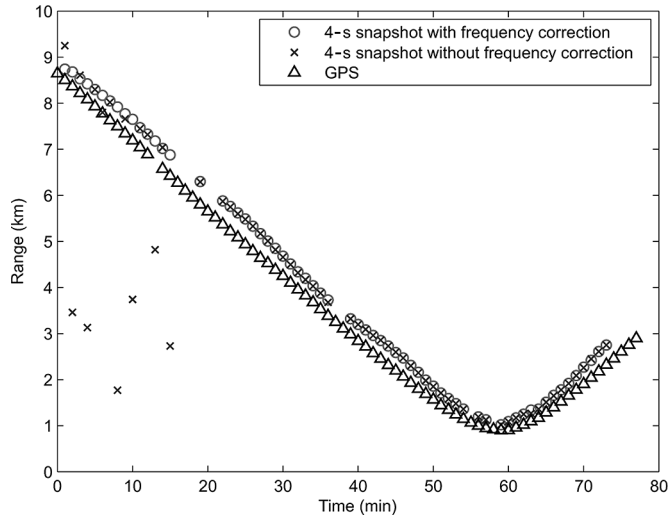

Fig. 5. Range trajectory estimated by the MFP-PDS processor using 4-s snapshots and 13 frequencies with and without the frequency correction.

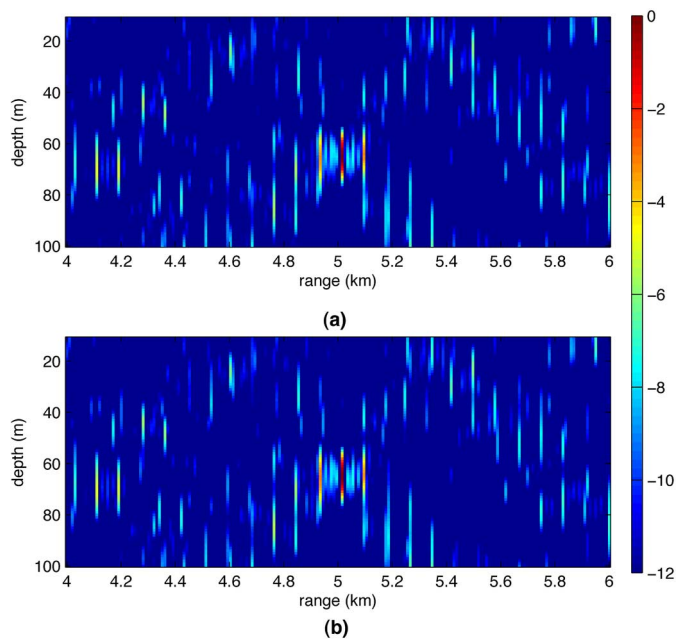

Fig. 6. Range–depth ambiguity surfaces computed by using (a) matched-phase coherent processor with PDS; (b) matched-phase coherent processor with ASSA. Five frequencies (hertz), 112, 130, 148, 166, 201, were processed in both processors. (The color bar is in logarithmic (decibel) scale. Each plot is normalized to its maximum value.)

To show the importance of frequency correction for locating the acoustic source, we applied the proposed MF processor to the experimental data with and without frequency correction. Fig. 5 shows the estimated range trajectories for the deep source by using the proposed MF processor with and without the frequency correction. The proposed MF processor was applied to the data collected in 4-s snapshots with 13 frequencies. With the 4-s snapshots, the frequency resolution is 0.25 Hz. With the ship speed of about 2.5 m/s, the maximum Doppler shifts are about 0.08 Hz for the lowest frequency (49 Hz) and about 0.64 Hz for the highest frequency (388 Hz). Without the frequency correction, the high frequencies only contribute noise, and thus, the MFP fails to locate the source at the beginning of the experiment, where SNR is low. Also, from Fig. 5, we see that, with frequency correction, the proposed MF processor always provides accurate localization even at the beginning of the experiment. In the remainder of this section, all simulation results were obtained with the frequency correction.

We also implemented the adaptive simplex simulated annealing (ASSA) algorithm proposed in [13] for computing the matched phases, and compared its performance and complexity with that of the MFP-PDS processor. For the ASSA algorithm, the following parameters were used: the initial temperature $T_0 = 0.5$; the temperature reduction factor is 0.98; the number of temperatures is 495. These values are optimized to provide a good performance with low complexity.

Figs. 6 and 7 show the ambiguity surfaces obtained by these two processors for 5 and 13 processed frequencies, respectively. We can see that the matched-phase processor with the PDS algorithm provides similar ambiguity surfaces as the matched-phase processor with ASSA: the peak-to-sidelobe ratios read from Fig. 6 for the processors are 3.16 and 3.17 dB, respectively. The peak-to-sidelobe ratios read from Fig. 7 are 6.59 and 6.55 dB, respectively. The matched phases obtained by using the two algorithms are listed in Table II. We see that the phases obtained by the PDS algorithm are very close to those obtained by the ASSA.

We compared the computational complexity of the PDS and ASSA algorithms by counting how many times the quadratic form $\mathbf{b}^H\mathbf{R}\mathbf{b}$ was computed. For each point in the location search grid, the quadratic form is computed once in each iteration of the algorithms, and this is the most computationally consuming part of the algorithms. These counts were averaged over the number of positions in the location grid. When processing five frequencies, the count for the ASSA algorithm is approximately 12 times of that of the PDS algorithm; specifically, they are 1399 and 116, respectively. When processing 13

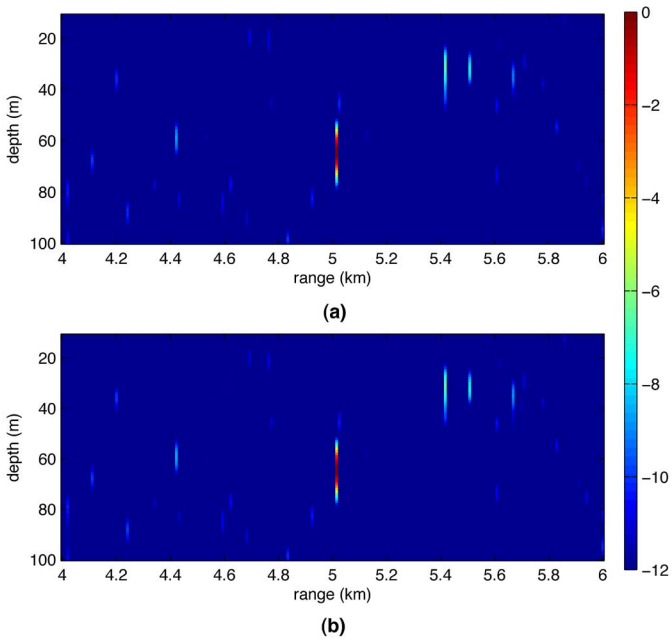

Fig. 7. Range–depth ambiguity surfaces computed by using (a) matched-phase coherent processor with PDS; (b) matched-phase coherent processor with ASSA. Thirteen frequencies (hertz), 49, 64, 79, 94, 112, 130, 148, 166, 201, 235, 283, 338, 388, were processed in both processors. (The color bar is in logarithmic (decibel) scale. Each plot is normalized to its maximum value.)

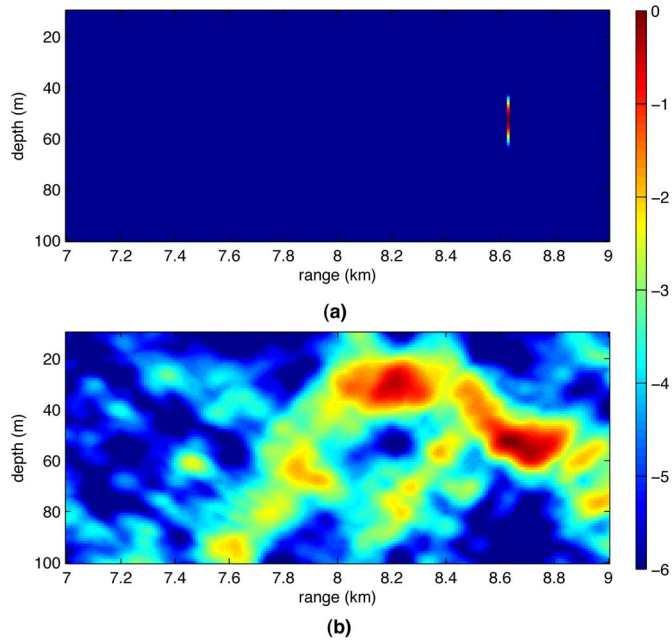

Fig. 8. Range–depth ambiguity surfaces computed by using (a) matched-phase coherent processor with PDS algorithm $B_M(\mathbf{x})$; (b) cross-frequency incoherent processor $B_X(\mathbf{x})$. (The color bar is in logarithmic (decibel) scale. Each plot is normalized to its maximum value.)

TABLE II
PHASE SHIFTS OBTAINED BY USING PDS AND ASSA ALGORITHMS

	Phase shifts (in degrees) with respect to the phase at frequency 112 Hz obtained for 5 processed frequencies
PDS	0, −90, 135, 45, −56
ASSA	0, −89, 140, 49, −48
	Phase shifts (in degrees) with respect to the phase at frequency 49 Hz obtained for 13 processed frequencies
PDS	0, 112, −124, 33, −56, −146, 78, −11, −112, −112, 90, 101, 157
ASSA	0, 108, −129, 29, −63, −156, 74, −16, −116, −118, 83, 97, 147

frequencies, the ratio is higher; the PDS algorithm computed the quadratic form 356 times, whereas the ASSA algorithm required 16 554 computations, i.e., the ASSA complexity was about 46 times of the PDS complexity. The difference is further increased as the number of processed frequencies increases.

Fig. 8(a) and (b) shows ambiguity surfaces obtained by the MFP-PDS processor and the cross-frequency incoherent processor [11], respectively. For both processors, 13 frequencies were used and one 1-s snapshot starting at the fourth minute of the experiment. The proposed processor provides the same peak level as the cross-frequency incoherent processor, which has been shown [11] to have the same maximum of the ambiguity surface as the matched-phase coherent processor using the simulated annealing method. It is seen that the cross-frequency incoherent processor gives a much wider peak in range and much higher sidelobes. The peak-to-sidelobe ratios read from Fig. 8(a) and (b) are about 6.1 and 0.3 dB, respectively.

Fig. 9 shows the range–depth ambiguity surfaces obtained by using the matched-phase coherent processor with the PDS algorithm for different numbers of processed frequencies. For Fig. 9(a), the middle five frequencies at 112, 130, 148, 166, and 201 Hz, as used in [10], were processed. For Fig. 9(b), the nine frequencies which had the highest SNR were processed. For Fig. 9(c), all 13 frequencies were used. A 1-s snapshot starting at the ninth minute of the experiment data was processed. We can see that, as the number of processed frequencies increases, the performance of the matched-phase coherent processor with PDS algorithm is improved. The peak-to-sidelobe ratios read from Fig. 9(a)–(c) are about 1.6, 5.5, and 6.3 dB, respectively.

Fig. 10 shows the range–depth ambiguity surfaces obtained by the matched-phase coherent processor with the PDS algorithm applied to a 1-s snapshot starting at the 30th minute of the experiment. White noise was added to the received signals to obtain SNRs: 15, 5, and −5 dB; corresponding ambiguity surfaces are shown in Fig. 10(a)–(c), respectively. The peak-to-sidelobe ratios read from these ambiguity surfaces are 8.5, 7.0, and 5.2 dB, respectively. Thus, the proposed processor can reliably locate the source at as low SNR as −5 dB.

Fig. 11 shows the range trajectory generated from the global positioning system (GPS) data recorded during the experiment [17] and the estimated range trajectories for the deep source by applying the matched-phase coherent processor with the PDS algorithm to the snapshots of different length. All the frequencies in the first set of tones were used for estimating the source trajectory. Due to the uncertainty about the correspondence of the starting time of the GPS measurements to the experiment data, the estimated range trajectories were shifted 1 min forward to better match the shape of the GPS measurements (the

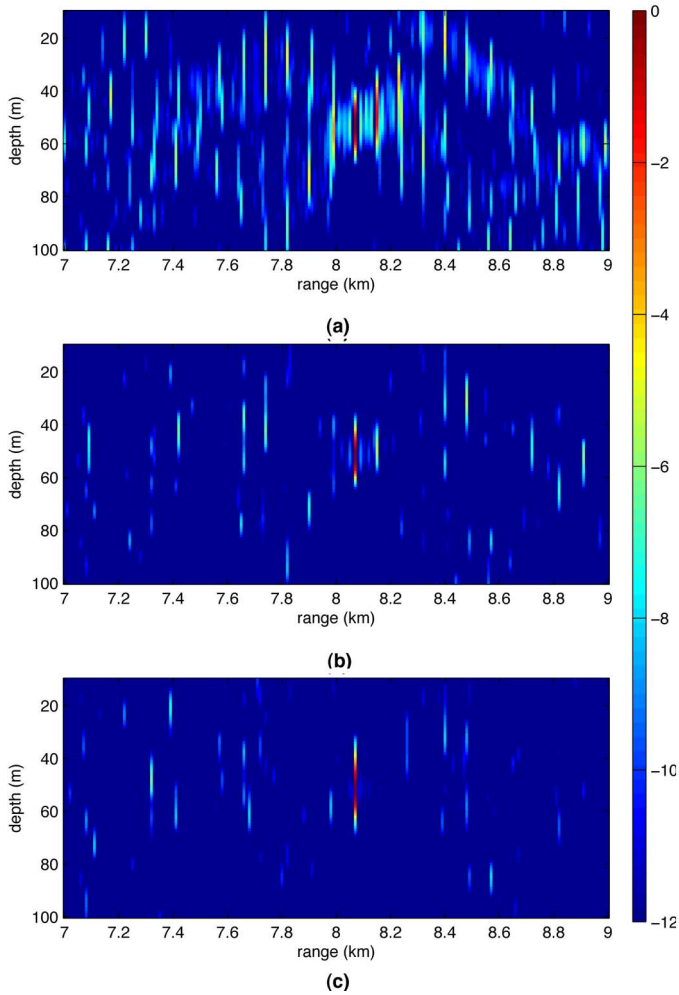

Fig. 9. Range–depth ambiguity surfaces computed by using matched-phase coherent processors with PDS algorithm, for different numbers of processed frequencies: (a) five frequencies (hertz): 112, 130, 148, 166, 201; (b) nine frequencies (hertz): 112, 130, 148, 166, 201, 235, 283, 338, 388; (c) 13 frequencies (hertz): 49, 64, 79, 94, 112, 130, 148, 166, 201, 235, 283, 338, 388. (The color bar is in logarithmic (decibel) scale. Each plot is normalized to its maximum value.)

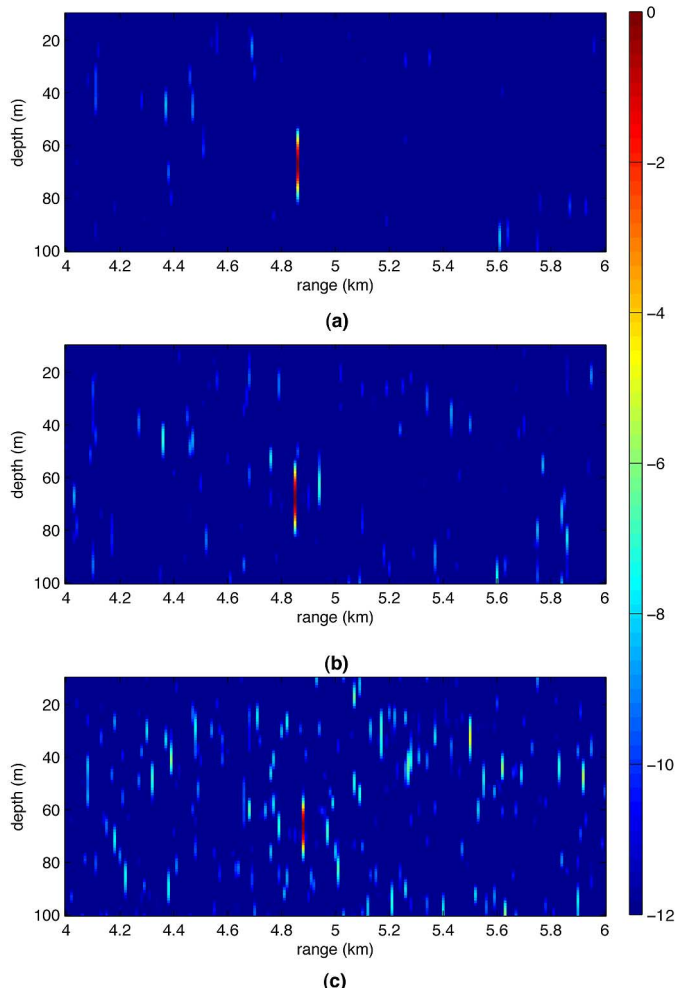

Fig. 10. Range–depth ambiguity surfaces computed by using the matched-phase coherent processor with PDS algorithm for different SNRs: (a) SNR $=$ 15 dB; (b) SNR $=$ 5 dB; (c) SNR $=-5$ dB. All 13 frequencies have been processed. (The color bar is in logarithmic (decibel) scale. Each plot is normalized to its maximum value.)

second minute of the experiment data corresponds to the first minute of the GPS measurements). Estimates of the range trajectories for those periods when the source stopped transmitting CW tones were removed. From Fig. 11, we see that with 0.25-s snapshots, the proposed matched-phase processor failed to locate the source in the first 20 min of the experiment and provided accurate localization afterward. We observe that the estimated trajectory obtained by applying the matched-phase processor to 1-s snapshots is well matched to the GPS measurements. This is because the SNR for the data collected in 0.25-s snapshot was much lower, especially when the source was far away from the receiver array. Further increase in the snapshot length allows accurate tracking the source as shown in Fig. 5 for 4-s snapshots. However, increase in the snapshot length affects the range resolution; e.g., with the source speed of 2.5 m/s, the range resolution for the 4-s snapshots is 10 m.

As can be seen from Fig. 11, shifts of around 50–400 m between the estimated trajectory and the GPS measurements are also observed. These shifts were probably caused by the mismatch in the bathymetry assumptions which were used for calculation of the replicas, as reported in [19] and [20]. These shifts are found to be very close to those shown in the comparison of ranges estimated by MFP with GPS measurements in [21] and [22].

Fig. 12 shows the depth trajectory obtained by the matched-phase coherent MF processor with the PDS algorithm. One-second snapshots with all the frequencies in the first set of tones were used. From Fig. 12, we see that the source fluctuated in depth between 50 and 75 m.

Finally, Fig. 13 shows how increase in the number of the processed frequencies improves the performance of the processor, thus justifying the need to have a computationally efficient algorithm for the phase search.

VII. Conclusion

In this work, we have reviewed the matched-phase coherent matched-field processor and introduced the PDS algorithm to the matched-phase coherent processor for searching the matched phases. The PDS algorithm is based on coordinate descent iterations with respect to the unknown phases and constrains the solution to have a unit magnitude. When compared

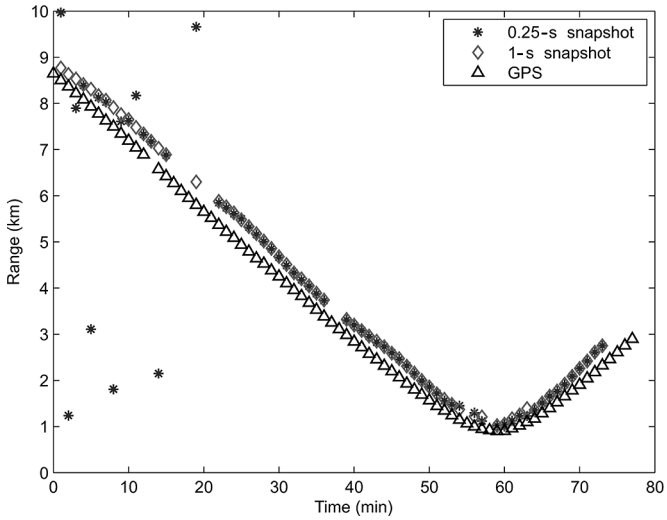

Fig. 11. Range trajectory obtained from GPS measurements and the estimated range trajectories for the deep source by applying the matched-phase coherent processor with PDS algorithm to the data collected in different snapshot lengths with 13 frequencies.

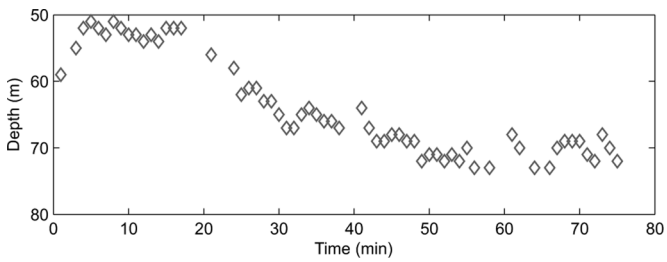

Fig. 12. Depth trajectory obtained by the MFP-PDS processor.

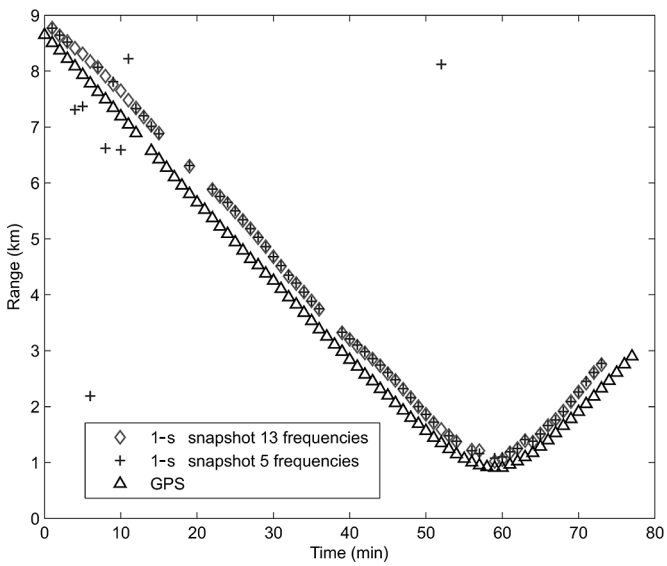

Fig. 13. Range trajectory obtained by the MFP-PDS processor with five and 13 processed frequencies.

with simulated annealing algorithm, it has significantly lower complexity, which enables simultaneous processing of many frequencies, and thus, improves processor performance.

The proposed processor has been applied to experimental data for source localization. It has been shown that, by using the proposed PDS algorithm, the matched-phase coherent processor can process more frequencies, and thus, gives better performance in reinforcing the main peak at the source location while reducing the sidelobes. The estimated range trajectory obtained by applying the processor to the data collected in every 1-s snapshot is well matched to GPS measurements.

REFERENCES

[1] H. P. Bucker, "Use of calculated sound fields and matched-field detection to locate sound sources in shallow water," *J. Acoust. Soc. Amer.*, vol. 59, pp. 368–373, 1976.

[2] E. K. Westwood, "Broadband matched-field source localization," *J. Acoust. Soc. Amer.*, vol. 91, pp. 2777–2789, 1992.

[3] N. O. Booth, P. A. Baxley, J. A. Rice, P. W. Schey, W. S. Hodgkiss, G. L. D'Spain, and J. J. Murray, "Source localization with broad-band matched-field processing in shallow water," *IEEE J. Ocean. Eng.*, vol. 21, no. 4, pp. 402–412, Oct. 1996.

[4] C. E. Lindsay and N. R. Chapman, "Matched field inversion for geoacoustic model parameters using adaptive simulated annealing," *IEEE J. Ocean. Eng.*, vol. 18, no. 3, pp. 224–231, Jul. 1993.

[5] N. R. Chapman and C. E. Lindsay, "Matched-field inversion for geoacoustic model parameters in shallow water," *IEEE J. Ocean. Eng.*, vol. 21, no. 4, pp. 347–354, Oct. 1996.

[6] A. B. Baggeroer, W. A. Kuperman, and H. Schmidt, "Matched field processing: Source localization in correlated noise as an optimum parameter estimation problem," *J. Acoust. Soc. Amer.*, vol. 83, no. 2, pp. 571–587, 1988.

[7] C. S. Clay, "Optimum time domain signal transmission and source location in a waveguide," *J. Acoust. Soc. Amer.*, vol. 81, pp. 660–664, 1987.

[8] L. N. Frazer and P. I. Pecholcs, "Single-hydrophone localization," *J. Acoust. Soc. Amer.*, vol. 88, pp. 995–1002, 1990.

[9] A. Tolstoy, "Computational aspects of matched field processing in underwater acoustics," *Comput. Acoust.*, vol. 3, pp. 303–310, 1990.

[10] G. J. Orris, M. Nicholas, and J. S. Perkins, "The matched-phase coherent multi-frequency matched-field processor," *J. Acoust. Soc. Amer.*, vol. 107, pp. 2563–2575, 2000.

[11] C. Soares and S. M. Jesus, "Broadband matched-field processing: Coherent and incoherent approaches," *J. Acoust. Soc. Amer.*, vol. 113, pp. 2587–2598, 2003.

[12] H. Szu and R. Hartley, "Fast simulated annealing," *Phys. Lett. A*, vol. 122, pp. 157–162, 1987.

[13] S. E. Dosso, M. J. Wilmut, and A. L. S. Lapinski, "An adaptive-hybrid algorithm for geoacoustic inversion," *IEEE J. Ocean. Eng.*, vol. 26, no. 3, pp. 324–336, Jul. 2001.

[14] Z. Quan, Y. V. Zakharov, and J. Zhang, "Multiple phase decoder for MIMO systems," in *Proc. 42nd Asilomar Conf. Signals Syst. Comput.*, Pacific Grove, CA, Oct. 26–29, 2008, pp. 1759–1762.

[15] Y. V. Zakharov and T. C. Tozer, "Frequency estimator with dichotomous search of periodogram peak," *Electron. Lett.*, vol. 35, no. 19, pp. 1608–1609, 1999.

[16] Y. V. Zakharov and T. C. Tozer, "Multiplication-free iterative algorithm for LS problem," *Electron. Lett.*, vol. 40, no. 9, pp. 567–568, 2004.

[17] J. Murray and D. Ensberg, "The Swellex-96 Experiment," [Online]. Available: http://www.mpl.ucsd.edu/swellex96/

[18] M. B. Porter, *The KRAKEN Normal Mode Program (Draft)*. Washington, DC: Naval Research Laboratory, 1992, vol. 22, pp. 71–127.

[19] G. L. D'Spain, J. J. Murray, W. S. Hodgkiss, N. O. Booth, and P. W. Schey, "Mirages in shallow water matched field processing," *J. Acoust. Soc. Amer.*, vol. 105, pp. 3245–3265, 1999.

[20] D. R. D. Balzo, C. Feuillade, and M. M. Rowe, "Effects of water-depth mismatch on matched-field localization in shallow water," *J. Acoust. Soc. Amer.*, vol. 83, pp. 2180–2185, 1988.

[21] P. Hursky, "Using ambient noise and sources of opportunity to estimate environment parameters and improve matched field source detection and localization," Ph.D. dissertation, Intell. Syst. Robot. Controls Group, Univ. California, San Diego, CA, 2001.

[22] Z. H. Michalopoulou, "Matched-impulse-response processing for shallow-water localization and geoacoustic inversion," *J. Acoust. Soc. Amer.*, vol. 108, pp. 2082–2090, 2000.

Teyan Chen graduated from the University of Central Lancashire, Preston, U.K., in 2005 and received the M.Sc. and Ph.D. degrees in electronic engineering from the University of York, York, U.K., in 2006 and 2011, respectively.

His research interests are in the areas of adaptive filtering, equalization, wireless communications, and underwater acoustic communications.

Chunshan Liu received the B.S. degree in physics from the University of Science and Technology of China, Hefei, China, in 2007 and the M.Sc. degree with distinction in communication engineering from the University of York, York, U.K., in 2008, where he is currently working towards the Ph.D. degree in electronic engineering.

His current research interests include adaptive array processing for underwater acoustics, signal processing for communications, and compressed sensing.

Yuriy V. Zakharov (M'01–SM'08) received the M.Sc. and Ph.D. degrees in electrical engineering from the Moscow Power Engineering Institute, Moscow, Russia, in 1977 and 1983, respectively.

From 1977 to 1983, he was an Engineer with the Special Design Agency, Moscow Power Engineering Institute. From 1983 to 1999, he was the Head of Laboratory at the N. N. Andreev Acoustics Institute, Moscow, Russia. From 1994 to 1999, he was with Nortel as a DSP Group Leader. Since 1999, he has been with the Communications Research Group, University of York, York, U.K., where he is currently a Reader. His interests include signal processing and communications.